Static analysis of beam structures using Refined 1D beam model

Personal programming project (PPP)
Winter semester 2019/2020

Arun Prakash Ganapathy

Mat.Nr. 63876

E-Mail: arun-prakash.ganapathy@student.tu-freiberg.de

Supervised by: Mr.Jeffy Abraham

Introduction

Beam structures are widely used in many engineering applications such as aircraft wings, helicopter blades, concrete beams in constructions etc., Classical 1-D models for beams made of isotropic materials are based on Euler-Bernoulli beam and Timoshenko theories. They yield better results for slender beams than short beams. If the cross-section of a bar is considered rigid, the problem can be considered as 1D one. In other words, the value of the displacement on the axis is enough to describe the deformation. But the classical 1D beam models do not take into the account of the non-classical effects like transverse shear deformation, torsion etc.,

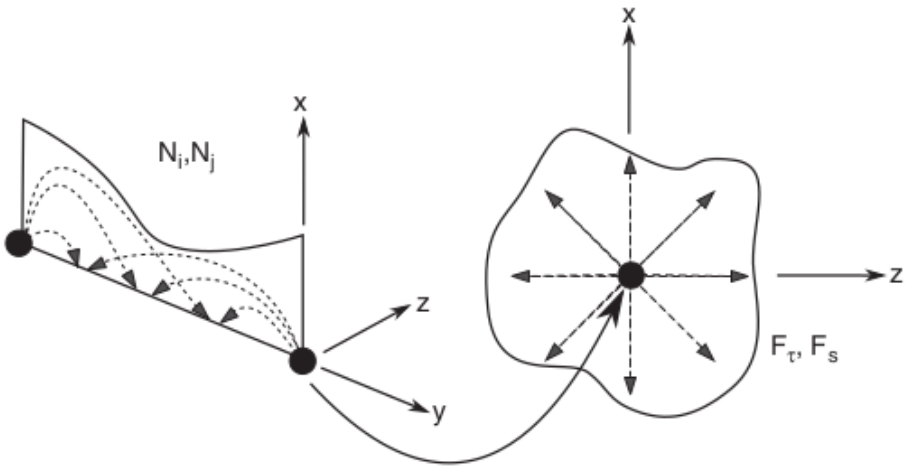

Figure 1: Refined 1D element based on CUF

To overcome this drawback, the displacement values, should not be considered constant over the cross-section. Rather the displacement that was originally defined in a 1D domain now becomes a 3D field. This can be done using Refined 1D beam models based on Carrera Unified Formulation (CUF). Refined 1D beam models use polynomial expansions (like Taylor, Lagrange polynomials etc.,) to approximate the displacement values across the cross-section of the beam. Therefore this theory requires two major steps for FEM implementation. 1. FE discretization on the axis of the beam element (1D) 2. Expansion across the cross-section (2D) using polynomials which gives the displacement field (See [2]). Refined theories are necessary to cope with unconventional cross-section geometries, short beams, orthotropic materials and non-homogenous sections. Figure (1) shows the axial approximation using 1D shape functions and cross-sectional approximation using polynomials.

Theory behind the Refined 1D Beam Model

1D Refined models with Lagrange Expansion class

In a displacement-based approach different class of functions are used to describe the displacement field of cross-section like harmonics, polynomials, exponentials etc., In this project, Lagrange polynomial expansion is used to approximate the displacement field of the cross-section. The Lagrange Expansion (LE) 1D models have the following main characters (See [2]),

- LE model variables and BCs can be located above the physical surfaces of the structure
- The unknown variables of the problems are only displacements of the nodes. No rotation or higher-order variables are used to describe the displacement field
- Locally refined models can be easily built since lagrange polynomial sets can be arbitrarily spread above the cross-section

In this method, the expansion functions (F_τ) coincide with the Lagrange polynomials. Since lagrange polynomials are usually given in normalized or natural coordinates the isoparametric formulation can be exploited. The simplest lagrange polynomial is the four-point (L4) set which is shown in the figure (2) and the polynomials are given (See [2]), in equation (1),

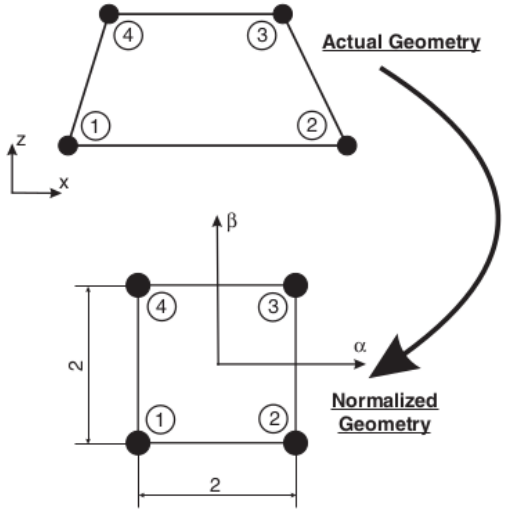

Figure 2: Four node Lagrange element(L4) in normalized and actual geometry

$$F_\tau = \frac{1}{4}(1+\alpha\alpha_\tau)(1+\beta\beta_\tau), \tau = 1,2,3,4 \tag{1}$$

where α and β are the normalized coordinates and α_τ and β_τ are the coordinates of the four nodes which is given in the table (1). In the same way triangular elements (L3) and higher-order elements like (L9) or (L16) can be created using their respective polynomials.

Point	α_τ	β_τ
1	-1	1
2	1	-1
3	1	1
4	-1	1

Table 1: Normalized coordinates of the four points of an L4 element

Isoparametic Formulation

Isoparametric formulation can be 1D, 2D or 3D. This formulation is used in refined 1D beam models to deal with

- 1D Shape functions are used along the longitudinal axis (Y) of the beam
- 2D expansion functions are used to describe the displacement field of the beam cross-section (X,Z)

The 2D isoparametric formulation is used to implement the LE models. The same 2D formulation is employed for the 2D FEs (Plate models)

Stiffness matrix

In CUF, the FE matrices (Stiffness and Mass matrix) are formulated in terms of Fundamental Nucleus (FN). The compact form of stiffness matrix (See [4]) is given by

$$\delta L_{int} = \delta \mathbf{u}_{sj}^T \mathbf{K}^{\tau sij} \mathbf{u}_{\tau i} \tag{2}$$

where $\mathbf{K}^{\tau sij}$ is the stiffness matrix written in the form of Fundamental Nucleus (FN). The FN is a $3 * 3$ array independent of the order of the structural model. The Nine components of the FN (See [2]) are given below

$$K_{xx}^{\tau sij} = C_{22} \int_A F_{\tau,x} F_{s,x} dxdz \int_l N_i N_j dy + C_{66} \int_A F_{\tau,z} F_{s,z} dxdz \int_l N_i N_j dy + C_{44} \int_A F_\tau F_s dxdz \int_l N_{i,y} N_{j,y} dy$$

$$K_{xy}^{\tau sij} = C_{23} \int_A F_\tau F_{s,x} dxdz \int_l N_{i,y} N_j dy + C_{44} \int_A F_{\tau,x} F_s dxdz \int_l N_i N_{j,y} dy$$

$$K_{xz}^{\tau sij} = C_{12} \int_A F_{\tau,z} F_{s,x} dxdz \int_l N_i N_j dy + C_{44} \int_A F_{\tau,x} F_{s,z} dxdz \int_l N_i N_{j,y} dy$$

$$K_{yx}^{\tau sij} = C_{44} \int_A F_\tau F_{s,x} dxdz \int_l N_{i,y} N_j dy + C_{23} \int_A F_{\tau,x} F_s dxdz \int_l N_i N_{j,y} dy$$

$$K_{yy}^{\tau sij} = C_{55} \int_A F_{\tau,z} F_{s,z} dxdz \int_l N_i N_j dy + C_{44} \int_A F_{\tau,x} F_{s,x} dxdz \int_l N_i N_j dy + C_{33} \int_A F_\tau F_s dxdz$$

$$\int_l N_{i,y} N_{j,y} dy$$

$$K_{yz}^{\tau sij} = C_{55} \int_A F_\tau F_{s,z} dxdz \int_l N_{i,y} N_j dy + C_{13} \int_A F_{\tau,z} F_s dxdz \int_l N_i N_{j,y} dy$$

$$K_{zx}^{\tau sij} = C_{12} \int_A F_{\tau,x} F_{s,z} dxdz \int_l N_i N_j dy + C_{66} \int_A F_{\tau,z} F_{s,x} dxdz \int_l N_i N_{j,y} dy$$

$$K_{yz}^{\tau sij} = C_{13} \int_A F_\tau F_{s,z} dxdz \int_l N_{i,y} N_j dy + C_{55} \int_A F_{\tau,z} F_s dxdz \int_l N_i N_{j,y} dy$$

$$K_{yy}^{\tau sij} = C_{11} \int_A F_{\tau,z} F_{s,z} dxdz \int_l N_i N_j dy + C_{66} \int_A F_{\tau,x} F_{s,x} dxdz \int_l N_i N_j dy + C_{55} \int_A F_\tau F_s dxdz \int_l N_{i,y} N_{j,y} dy$$

Load Vector

The virtual variation of the external work due to load P is given by the equation (3) below (See [3])

$$\delta L_{ext} = P \delta u^T \tag{3}$$

By introducing nodal displacements and shape functions for the refined beam model the above equation becomes

$$\delta L_{ext} = F_\tau N_i P \delta u_{\tau i}^T \tag{4}$$

The above equation helps us to assemble the load vector by detecting the displacement variables that have to be loaded. In case of a first-order Taylor expansion across the cross-section and a load P acting on X-direction only the virtual work is given by (See [3]),

$$\delta L_{ext} = P_{u_x} \delta u_{x1} + x_P P_{u_x} \delta u_{x2} + z_P P_{u_x} \delta u_{x3} \tag{5}$$

where $[x_P, z_P]$ are the coordinates on the cross-section of the loading application point.

Numerical methods and Implementation

The computation of FN requires the evaluation of surface integrals in the cartesian coordinates (X and Z) (See [2])

$$\int_A F_{\tau,x} F_{s,x} dxdz$$

where the 2D integration domain (A) can be of arbitrary shape. If normalized coordinates are used (α and β) the integral can be computed above the fixed 2D domain instead of the actual geometry. For example, if quadrilateral elements are used the integral becomes

$$\int_A F_{\tau,x}(x,z) F_{s,x}(x,z) dxdz = \int_{-1}^{+1} \int_{-1}^{+1} F_{\tau,x}(\alpha,\beta) F_{s,x}(\alpha,\beta) |J(\alpha,\beta)| d\alpha d\beta$$

where $|J|$ is the Jacobian of the transformation. The Jacobian can be obtained form the following relation (See [2])

$$F_{\tau,\alpha} = F_{\tau,x}\ x_\alpha + F_{\tau,z}\ z_\alpha$$

$$F_{\tau,\beta} = F_{\tau,x}\ x_\beta + F_{\tau,z}\ z_\beta$$

It can be rewritten in the matrix form

$$\begin{Bmatrix} F_{\tau,\alpha} \\ F_{\tau,\beta} \end{Bmatrix} = \overbrace{\begin{bmatrix} x_\alpha & z_\alpha \\ x_\beta & z_\beta \end{bmatrix}}^{\text{Jacobian matrix}} \begin{Bmatrix} F_{\tau,x} \\ F_{\tau,z} \end{Bmatrix}$$

Derivatives inside the Jacobian matrix takes the form

$$x_\alpha = F_{1,\alpha}\ x_1 + F_{2,\alpha}\ x_2 + F_{3,\alpha}\ x_3 + F_{4,\alpha}\ x_4$$

$$z_\beta = F_{1,\beta}\ z_1 + F_{2,\beta}\ z_2 + F_{3,\beta}\ z_3 + F_{4,\beta}\ z_4$$

Gauss quadrature for numerical integration

The integrals in the FN components have an analytical solution but in practice, numerical integration is used. Gauss quadrature is extensively used in FEA for numerical integration purposes. Gauss quadrature approximates the definite integral of a function by taking a weighted sum of a function at specified points within the domain of integration. For example, the 1D integration in the FN nucleus is approximated by

$$\int_{-1}^{1} N_i N_j |J|\ d\xi = \sum_h w_h\ N_i(\xi_h)\ N_j(\xi_h)\ |J(\xi_h)|$$

where w_h is the integration weight and ξ_h is the integration point. The 2D integration in the FN is approximated as shown below (See [2])

$$\int_{-1}^{1}\int_{-1}^{1} F_\tau F_s |J| d\alpha d\beta = \sum_{h,k} w_h\ w_k\ F_\tau(\alpha_h,\beta_k) F_s(\alpha_h,\beta_k) |J(\alpha_h,\beta_k)|$$

where w_h, w_k are the integration weights and α_h, β_k are the integration points. The number of gauss points required for certain integral is given by the relation $k = 2n_p - 1$ where k is the order of integration and n_p is the number of gauss points. For example, the gauss points and weights for 1D and 2D integration using 2 gauss points is given the tables (2) and (3) (See [2]) below

Implementation

Stiffness matrix

In CUF, the stiffness matrix is computed in terms of FN. The FN is a 3*3 matrix whose nine components are given in the equation. Four indices are used to assemble

ξ_h	w_h
0.57735	1
-0.57735	1

Table 2: Integration points and weights for 1D integration

α_h	β_k	w_h	w_k
0.57735	0.57735	1	1
0.57735	-0.57735	1	1
-0.57735	0.57735	1	1
-0.57735	-0.57735	1	1

Table 3: Integration points and weights for 2D integration

the stiffness matrix (τ, s, i, j). τ, s are related to the expansion functions F_τ and F_s and the FN is computed by varying τ and s. The block computed by varying τ and s is called the nodal stiffness matrix. The element stiffness matrix is then computed by assembling the nodal stiffness matrix by varying i and j. After that global stiffness matrix is obtained by assembling the element stiffness matrix of each element using the appropriate assignment matrix. The process of assembling a global stiffness matrix is shown in the figures (3), (4) and (5) below (See [2])

The graphical description (Pseudocode) of the process of assembling stiffness matrix is given in the figure (6) below (See [2]). Since L4 Polynomials are used, instead of having a single node as if in 1D FEM each node will have four nodal points (beacause of the L4 expansion). Therefore a single B2 (Linear) element has 8 nodes and each node has 3 degrees of freedom (DOF). As a result of that, each B2 element will have 24*24 element stiffness matrix (8*3). This gets more complex if B3 (36*36 matrix) and B4 (48*48 matrix) elements are used for the analysis. Therefore appropriate assignment matrix has to be computed for each case to assemble the element stiffness matrix to get global stiffness matrix.

Load Vector

The Load Vector for any type of loading can be derived from equation (4). Let us consider a B2 element having a square cross-section loaded by a downward force P (Z-direction) at the central point of the tip cross-section (Cantilever beam). The Load vector is computed by the PVD

$$\delta L_{ext} = F_\tau N_i P \delta u_{\tau i}^T \tag{6}$$

The value of the shape function at the loading point is 1 and at the fixed end, it is zero. Therefore $N_1 = 0$ and $N_2 = 1$. P acts in z-direction therefore only u_z components of the load vector is involved. Therefore the virtual variation of the external work is given by

$$\delta L_{ext} = PF_1 u_{z_{11}} + PF_2 u_{z_{12}} + PF_3 u_{z_{13}} + PF_4 u_{z_{14}}$$

By substituting the value of the natural coordinates (α, β) of the loading position (0,0) in the Lagrange polynomials of the above equation we get

$$\delta L_{ext} = \frac{P}{4} u_{z_{11}} + \frac{P}{4} u_{z_{12}} + \frac{P}{4} u_{z_{13}} + \frac{P}{4} u_{z_{14}}$$

According to the above equation, a load of magnitude $\frac{P}{4}$ has to be placed in the 3,6,9 and 12th position of the nodal load vector.

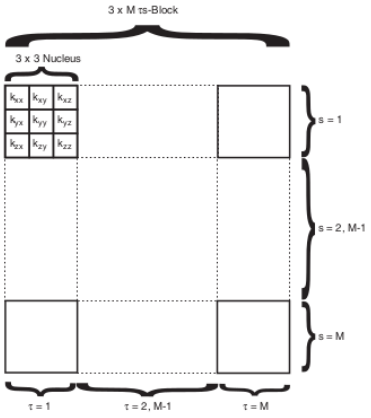

Figure 3: Nodal stiffness

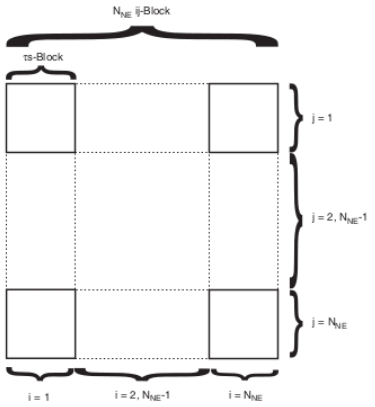

Figure 4: Element stiffness

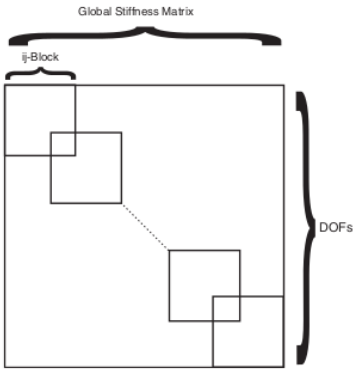

Figure 5: Global stiffness

Postprocessing (Displacements,Stresses and Strains)

From the displacement values obtained from the analysis, strain and stress values at the point of interest can be obtained. To do that the displacement values are expanded over all the points where post-processing is needed. This expansion can be done with the help of shape functions. The shape functions $(N_i(y))$ along the beam axis and expansion functions (F_τ) above the cross-section. The equation for expansion is shown in the equation below (See [2])

$$u_x(x_p, y_p, z_p) = N_i(y_p) F_\tau(x_p, z_p) u_{x_{\tau i}} \tag{7}$$

$$u_y(x_p, y_p, z_p) = N_i(y_p) F_\tau(x_p, z_p) u_{y_{\tau i}} \tag{8}$$

$$u_z(x_p, y_p, z_p) = N_i(y_p) F_\tau(x_p, z_p) u_{z_{\tau i}} \tag{9}$$

where $[x_p, y_p, z_p]$ is a generic point of the structure where the displacement values have to be computed. The terms $[u_{x_{\tau i}}, u_{y_{\tau i}}, u_{z_{\tau i}}]$ are the x, y and z displacements of the nodal points computed from the FE Analysis. Stress and strain components are straightforwardly computed from the nodal displacement values. To find the strains, partial derivatives are required which can be calculated utilizing shape and expansion functions.

$$u_{,x} = (F_\tau N_i u_{\tau i})_{,x} = F_{\tau,x} N_i u_{\tau i} \tag{10}$$

$$u_{,y} = (F_\tau N_i u_{\tau i})_{,y} = F_\tau N_{i,y} u_{\tau i} \tag{11}$$

$$u_{,z} = (F_\tau N_i u_{\tau i})_{,z} = F_{\tau,z} N_i u_{\tau i} \tag{12}$$

As the strain field is computed, stress components are obtained through the constitutive laws

$$\{\sigma\} = [C]\,\{\epsilon\} \tag{13}$$

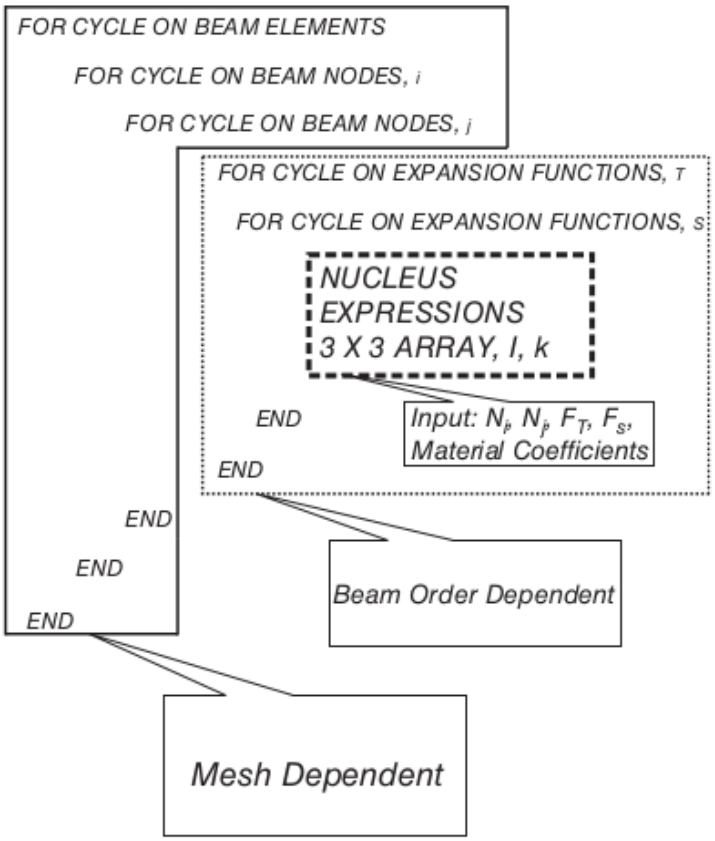

Figure 6: Graphical description of the FN implementation

Results and Discussion

Beams subjected to bending loads are analyzed here using refined 1D beam models. Clamped boundary conditions are accounted for the analysis. The beams are

considered to have a conventional square cross-section and an unconventional elliptical cross-section. An isotropic material of Young's modulus(E) 75 [GPa] and Poisson's ratio, 0.33, is used for both the cases.

Inital Tests

Before analyzing the above-mentioned cross sections, two fundamental tests has been conducted in order to test the functionality of the code. The tests are stiffness matrix test and tension test.

Stiffness matrix test

In order to check whether the stiffness matrix derived using the Fundamental Nucleus (FN) technique (a rather new approach) works well, one of the components of the stiffness matrix derived for a particular case using analytical solution presented in the literature has been compared with the same component for the same case obtained using the implemented code. The test case is given as follows: A rectangular beam of length L is considered. A B2 element is used along the beam axis and an L4 element is adopted across the cross-section. The analytical solution for the (15*3) component of the element stiffness matrix is given below (See [2])

$$k_{xx}^{2122} = \frac{1}{18}\frac{bL}{a}C_{22} + \frac{1}{18}\frac{aL}{b}C_{66} - \frac{4}{9}\frac{ab}{L}C_{44} \tag{14}$$

For a square cross-section beam of length L = 2m, cross section of a = b = 0.2m and elastic constants (C_{22}, C_{44}, C_{66}) for the above given isotropic material the obtained value of the above component is $1.544 * 10^{10}$. The value of the same 15*3 component of the element stiffness matrix obtained using the implemented code is $1.522 * 10^{10}$. This proves that the implemented code complies well with the analytical solution.

Tension test

Since refined 1D beam models are generalized models, tension test can be carried out by deriving appropriate load vector which applies the load in the positive y-direction (along beam axis). And also the exact solution for calculating the deformation due to tensile load can be easily derived, it serves as a viable candidate to check whether the displacement obtained from the implemented code is correct or not. The deformation due to tensile load is given by

$$sdL = \frac{PL}{EA} \tag{15}$$

where P - load applied, L - length of the beam, A - area of cross-section and E - Young's modulus. For a load of 50N and a beam of above-given parameters the deformation due to the load P, is found to be $3.3 * 10^{-8} m$. The Load vector for tension load (used in code) can be derived using the equation (6) by applying the load in positive y-direction. The deformation calculated by the implemented code (using 20 B2 elements) due to a tensile of 50N is found to be $2.96 * 10^{-8}$. This proves that the deformation obtained using the implemented model is close enough to the exact solution.

Square cross-section beam:

A cantilever beam of square cross-section undergoing a vertical force, P_{u_z}, is considered for the analysis. A load (P_{u_z}) of -50[N] is applied at the central point of the tip cross-section in order to perform typical bending analysis. The sides of section (a) are equal to 0.2[m]. The span to height ratio $\frac{L}{h}$ is equal to 10. The mechanics of the beam is described in terms of the maximum vertical displacement (u_z) computed at the central point of the tip cross-section and the maximum absolute value of axial strain and stress. A reference solution for the above-given terms is given as follows (See [1]),
Maximum vertical displacement

$$u_z = \frac{P_{u_z} L^3}{3EI} \tag{16}$$

Absolute value of maximum strain

$$\epsilon_{yy} = \frac{P_{u_z} Lh}{2EI} \tag{17}$$

Absolute value of maximum stress

$$\sigma_{yy} = \frac{P_{u_z} Lh}{2I} \tag{18}$$

Maximum vertical displacement (u_z):

Tables (4), (5) and (6) presents the maximum vertical displacement, u_z, computed using Linear (B2), Quadratic (B3) and Cubic (B4) elements respectively along the beam axis. L4 expansion is used across the cross-section for all the cases and a span to height ratio of 10 is used. The reference solution for maximum vertical displacement, u_z, obtained using the formula (16) is $-1.333 * 10^{-5}$ $[m]$. From the tables, it is evident that the accuracy of the displacement values increases with increase in the number of elements along the beam axis. Because higher number of elements increases the flexibility of the structure. In the case of linear elements, the model converges to a maximum displacement of only $-0.9 * 10^{-5}$ $[m]$ as seen from the table (4).

No of elements	$u_z * 10^5$ $[m]$
1	-0.68
2	-0.85
10	-0.90
20	-0.90
40	-0.90

Table 4: Displacement values (u_z) obtained using B2 element

The accuracy of the model can be increased by changing the type of element. Table (5) presents the value of maximum vertical displacement computed using Quadratic element. The model predicts a displacement of $-0.9499 * 10^{-5}$ $[m]$ in the beginning and converges to a maximum displacement of $-1.283 * 10^{-5}$ $[m]$ which is pretty close to the reference solution.

No of elements	$u_z * 10^5$ $[m]$
1	-0.949
2	-1.224
10	-1.286
20	-1.283
40	-1.283

Table 5: Displacement values obtained (u_z) using B3 element

Table (6) presents the maximum vertical displacement obtained using the Cubic element (B4). The model predicts a displacement of $-0.9088 * 10^{-5}$ $[m]$ initially and it stays at the same value even if the number of elements is increased. The cubic element is supposed to be more accurate than quadratic element, on contrary it stays at the same value. The problem could be due to the fact that the cubic element might not work well with L4 polynomial expansion across the cross-section. Therefore, higher-order polynomials like L9 or L16 has to be implemented in order to make cubic element models more accurate.

No of elements	$u_z * 10^5$ $[m]$
1	-0.908
2	-0.908
10	-0.908
20	-0.908
40	-0.908

Table 6: Displacement values obtained (u_z) using B4 element

Therefore, it can be concluded that the quadratic beam element has the potential to yield more accurate results provided that L4 polynomial expansion is used across the cross-section.

The comparison of vertical displacements (u_z) of the central point of the tip cross-section for different beam elements is shown in Fig.7. 1, 2, 10, 20, 40 number of elements are considered for the comparison. Fig (8) shows the Z displacement of the

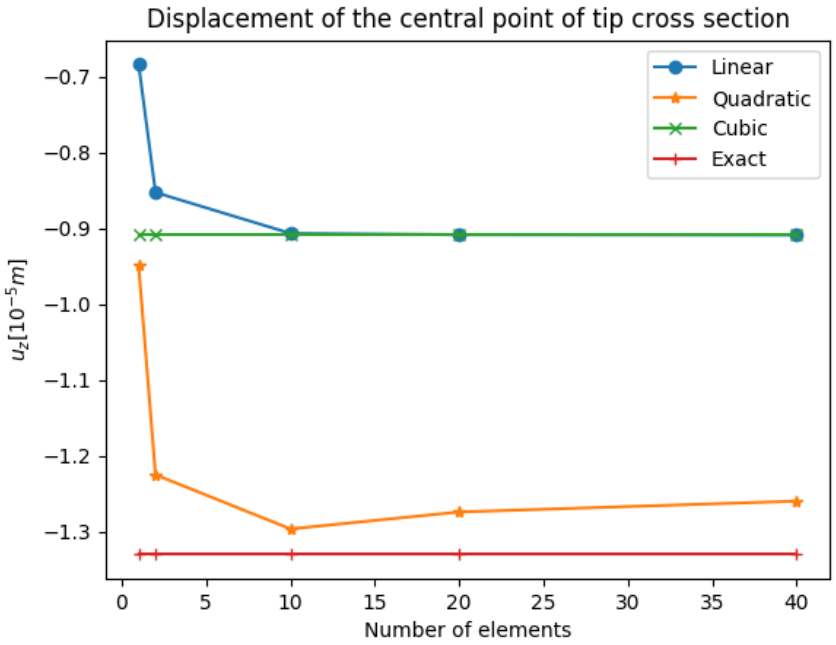

Figure 7: u_z vs number of beam elements for different type elements

central point of all cross-sections of the beam. It shows the typical bending behaviour of the beam. The displacements are computed using 20 B3 elements along the beam axis and L4 polynomials across the cross-section.

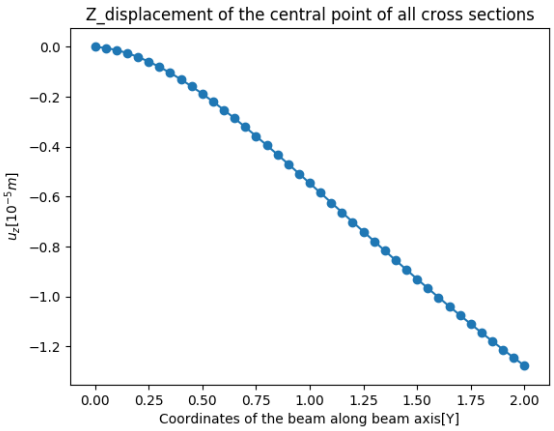

Figure 8: Displacement (u_z) of the beam using 20 B3 elements

Maximum axial strain and stress (ϵ_{yy}, σ_{yy}):

The main aim of the refined 1D beam model is to predict the 3D behaviour of the beam when subjected to loading. With the help of X, Y and Z displacements, strains and stresses at any point in the beam can be computed using the equations (10), (11) and (12). Since vertical load is applied in the beam, X displacement becomes zero so it can be neglected. The maximum axial strain and stress given by the equations (17) and (18) serves as a reference solution for comparing the stresses and strains computed by our model. Since maximum axial strains and stresses are present in the fixed end, it can be computed with the help of Y displacements of the cross-section close to the fixed end. With the help of displacements, shape functions and equation (11), axial strain (ϵ_{yy}) at any point in the cross-section can be computed. Fig (9), presents the variation of axial strain above the cross-section at the fixed end computed using 40 B3 elements along the beam axis and a 50*50 meshgrid.

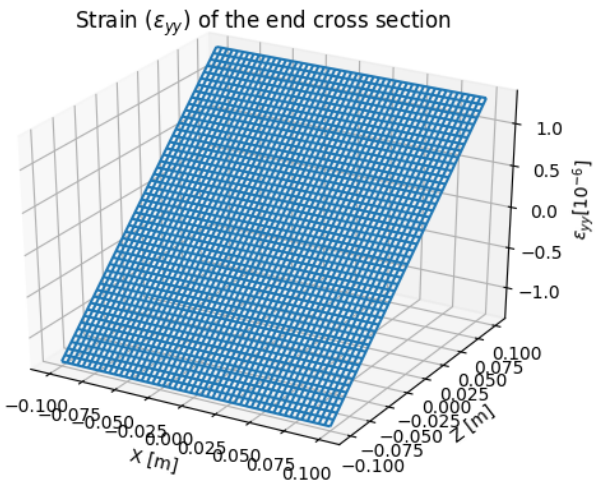

Figure 9: Axial strain (ϵ_{yy}) above the cross-section at y=0

Table (7) presents the absolute value and the position of maximum axial strains and stresses computed at the fixed end (Y=0) using different type of elements. The position of maximum stresses and strains does not depend on x. It is observed from the table that maximum stress and strain computed using B2 and B3 elements agrees well with the reference solution. But the values computed using the B4 element does not matches well because of the fact that the B4 element requires higher-order expansion across the cross-section to increase its accuracy. Fig (10) and (11) presents the variation in the axial strain and stress versus z at x = y = 0.

Type of element	$\epsilon_{zz} * 10^6$	$\sigma_{zz}\ [MPa]$	**x**	**y**	**z**
Ref soln	1.000	0.075	$-\frac{b}{2} \leq +\frac{b}{2}$	$\pm\frac{h}{2}$	0
B2	1.333	0.099	$-\frac{b}{2} \leq +\frac{b}{2}$	$\pm\frac{h}{2}$	0
B3	1.333	0.099	$-\frac{b}{2} \leq +\frac{b}{2}$	$\pm\frac{h}{2}$	0
B4	0.448	0.033	$-\frac{b}{2} \leq +\frac{b}{2}$	$\pm\frac{h}{2}$	0

Table 7: Maximum axial strains and stresses computed using different type of elements)

From fig (10), it is observed that B2 and B3 beam elements produce almost the same strain values and they are close to the reference solution. But the values computed by B4 element is not close to the reference solution. The same can be observed for the fig (11) which shows the axial stress vs y at x = y = 0.

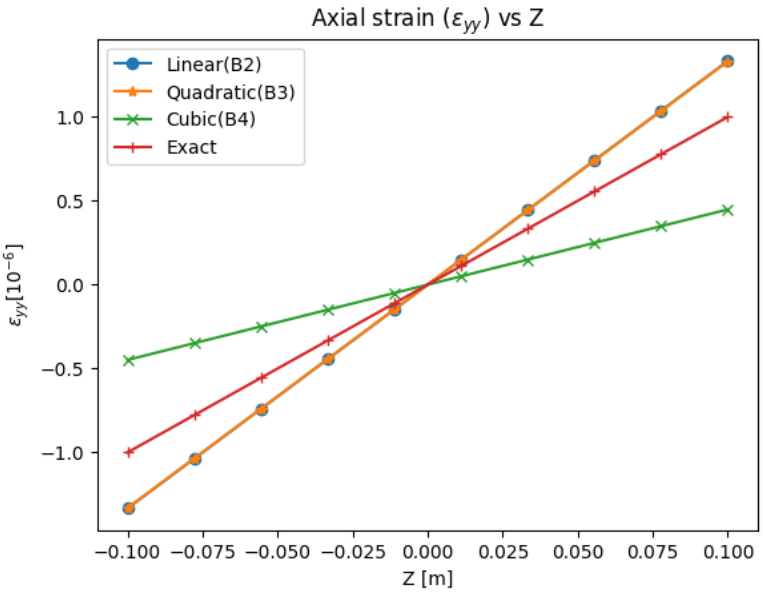

Figure 10: Axial strain (ϵ_{yy}) vs z at x=0 and y=0. 40 beam elements.

With the maximum stress and strain verified using the reference solution, the distribution of strains and stresses at any point in the beam can be found out using the displacement values obtained at the nodes and shape functions. Figure (12) and (13) shows the distribution of axial strains and stresses at the cross-section close to the fixed end.

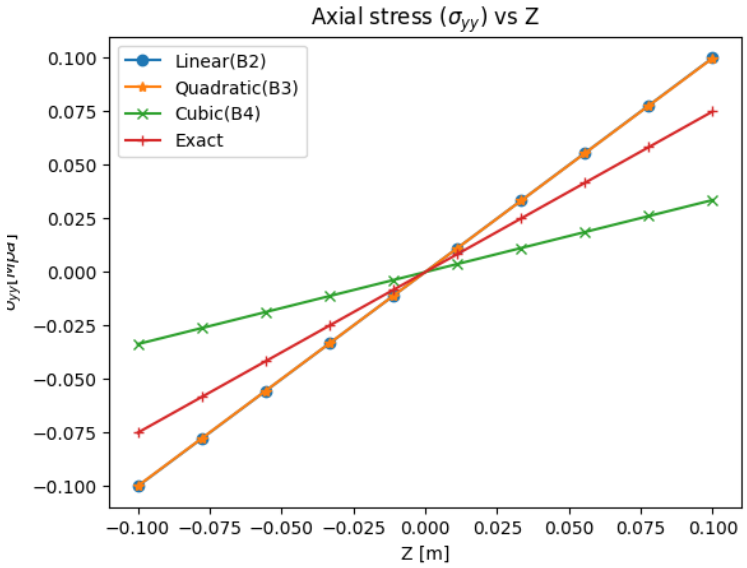

Figure 11: Axial stress (σ_{yy}) vs z at x=0 and y=0. Type of element:B4. 40 beam elements.

This distribution of strains and stresses are obtained by computing strain values at all the points in a 50*50 meshgrid by interpolation of strains with the help of displacements and shape functions.

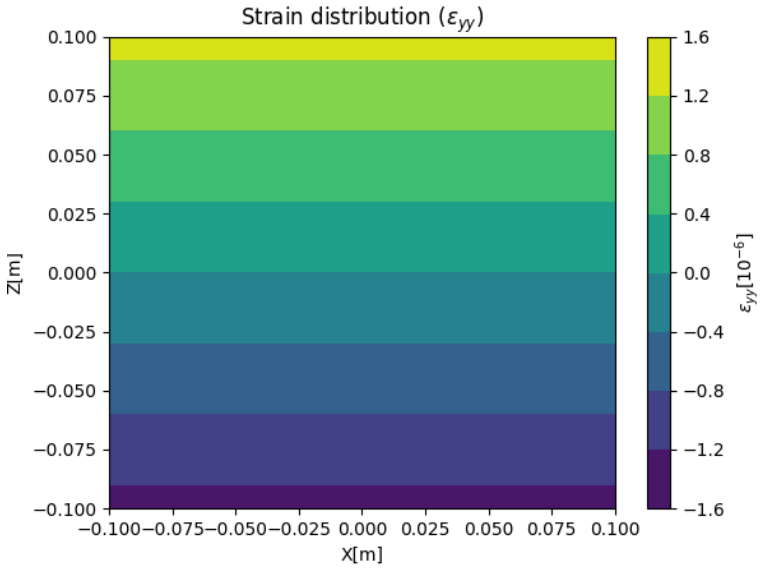

Figure 12: Distribution of strain at the fixed end cross-section (ϵ_{yy})

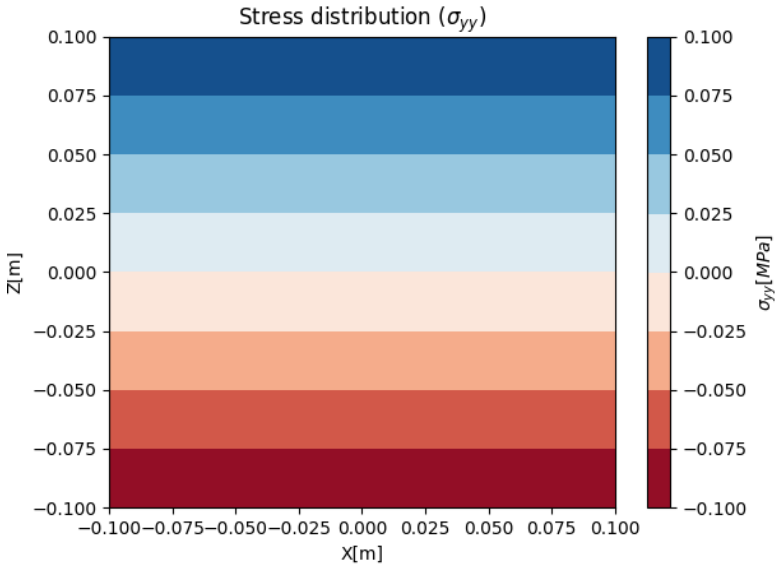

Figure 13: Distribution of stress at the fixed end cross-section (σ_{yy})

In order to check whether the implemented model can be applied for practical applications, a NASTRAN model has been built for the comparison purpose. Fig (14) presents the NASTRAN model which shows the distribution of axial stress (σ_{yy}). It is observed from the figure that it shows a stress range of -0.0905 [MPa] to 0.0916 [MPa]. This close enough to our implemented model where the stress ranges from -0.1 [MPa] to 0.1 [MPa] as seen the figure (13).

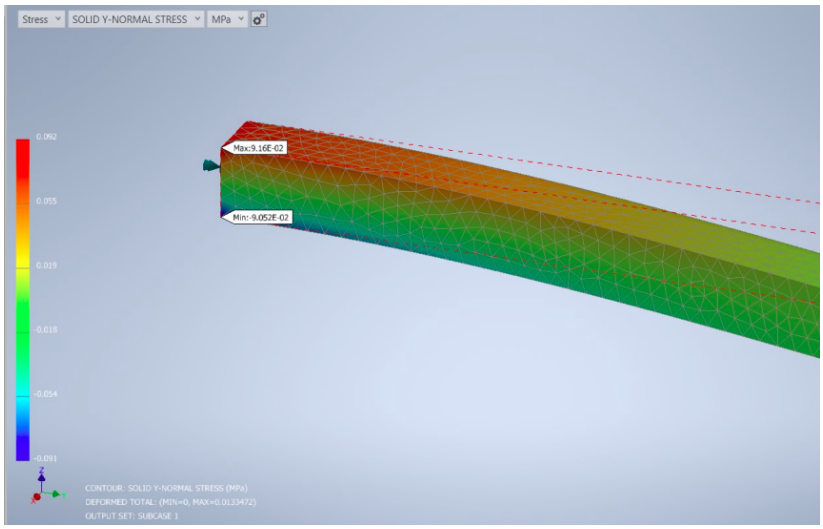

Figure 14: NASTRAN model showing the distribution of axial stress (σ_{yy})

Y displacement of the tip cross-section:

Y displacement of the tip cross-section gives a better understanding of the tilting behaviour of the end cross-section visually which cannot be obtained from classical beam models like Euler-Bernoulli. Y displacement of the nodes of end cross-section and shape functions are used to interpolate the displacement values across the whole cross-section using 50*50 meshgrid.

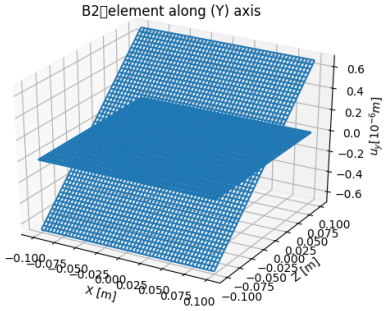

Figure 15: B2 element along Y axis

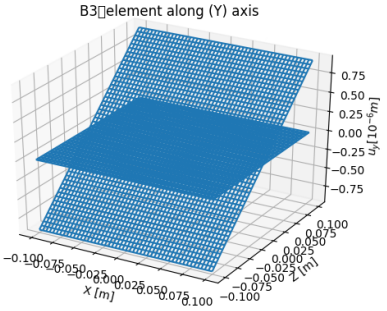

Figure 16: B3 element along Y axis

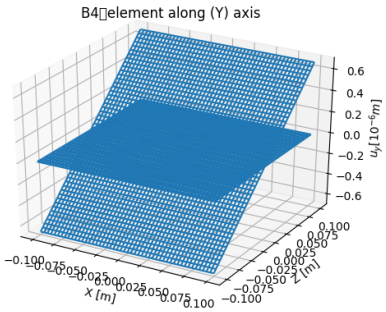

Figure 17: B4 element along Y axis

Figure (15), (16) and (17) shows the tilt of end cross-section with respect to the undeformed cross-section computed using 40 B2, B3 and B4 elements respectively. Table (8) shows the comparison of peak Y displacements computed using our implemented model and the NASTRAN model. It is observed from the table that the accuracy of the solution increases with changing the type of element and the displacement computed using B3 element is pretty much close to the NASTRAN model. Since the B4 element does not work well with the L4 polynomial the maximum displacement obtained is same as that of B2 element. This approach can be further extended to non-classical effects such transverse shear deformation, torsion etc., by deriving appropriate load vector. And also by employing higher-order Lagrange polynomials like (L9) or (L16), the behaviour of the cross-section can be characterised more accurately.

Element type	$u_y * 10^7$ $[m]$
NASTRAN sol.	9.99
B2	6.74
B3	9.31
B4	6.74

Table 8: Displacement (u_y) computed using type of elements. No of elements 40.

Elliptical Cross-section:

Refined 1D beam model can be extended to any beam structures of the arbitrary cross-section with the help of expansion functions across the cross-section. In order to check the ubiquity of our model an elliptical cross-section has been chosen. Clamped boundary conditions are accounted for the analysis. The length of the beam is 4[m] and the major and minor axes are 0.8 and 0.4[m] respectively. A vertical force (P_{u_z}) of -100[N] is applied at the central point of the tip cross-section. The elliptical cross-section is modelled by fitting a maximum possible rectangle inside the ellipse and analysed using appropriate jacobian value. Since we have no reference solution for elliptical cross-section beam a NASTRAN model has been built for the comparison purposes. The table (9) below shows the comparison of maximum vertical displacement of the NASTRAN model and the model built using different type of elements (For 40 elements). It is observed from the table that the model behaves as same for square cross-section. The accuracy of the model is high with the B3 element and the maximum displacement of the B4 element is same as that of B2.

Element type	$u_z * 10^7$ $[m]$
NASTRAN sol.	-7.08
B2	-5.84
B3	-8.01
B4	-5.84

Table 9: Displacement (u_z) computed using type of elements. No of elements 40.

Figure (18) presents the Z displacement of the central point of all cross-sections computed using 40 B3 elements which shows the bending behaviour of the beam.

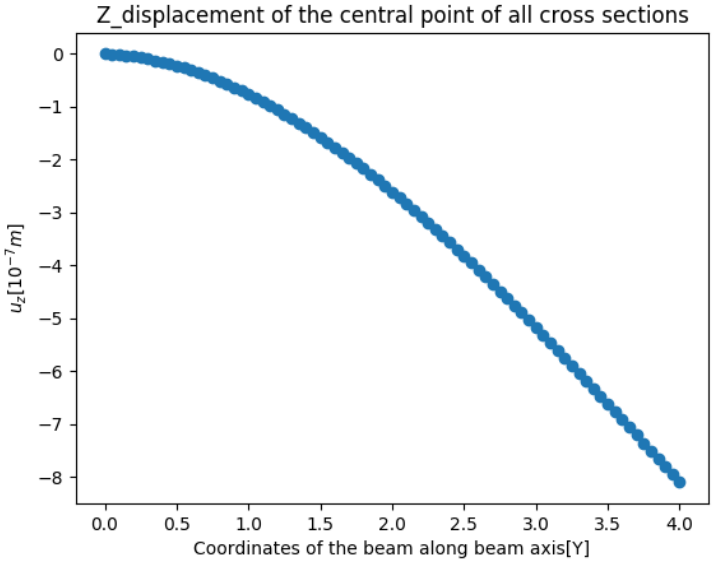

Figure 18: Dislacement (u_z) computed using 40 B3 elements

Y displacement of the tip cross-section helps us to visualize the tilting behaviour of the beam cross-section. The cross-section here is constructed with a 100*100 mesh grid of side length equal to the major axis and then excluding the grid points which are not in the ellipse with the help of the equation of the ellipse. The formula (19) shows the equation of the ellipse

$$\frac{x^2}{a^2} + \frac{y^2}{b^2} = 1 \tag{19}$$

where x and y are the coordinate points and a and b are the semi-major and semi-minor axis respectively. Table (10) shows the comparison of peak Y displacement of the NASTRAN model and our model computed using different type of elements. It is observed that the model behaves as same as that of square cross-section where B3 is more accurate and B2 and B4 are same.

Element type	$u_y * 10^7$ $[m]$
NASTRAN sol.	1.05
B2	0.84
B3	1.15
B4	0.84

Table 10: Peak displacement (u_y) computed using type of elements. No of elements 40.

Fig (19), (20) and (21) presents the y displacement of the end cross-section which gives a visualization of how the beam cross-section tilts when loaded with a vertical force of -100 [N].

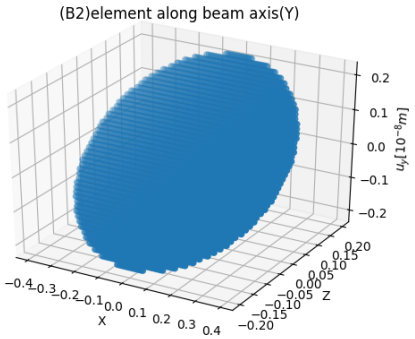

Figure 19: B2 element along Y axis

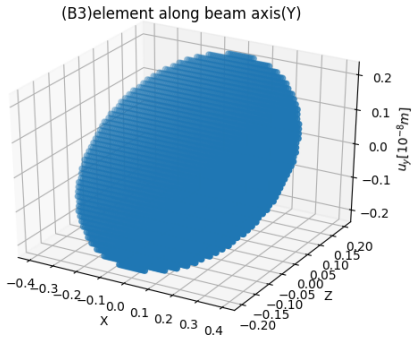

Figure 20: B3 element along Y axis

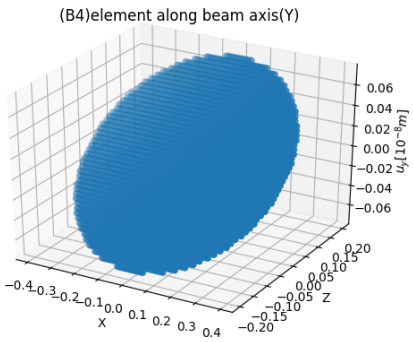

Figure 21: B4 element along Y axis

The distribution of strains and stresses are obtained by computing strain values at all the points in a 100*100 meshgrid by interpolation of strains with the help of displacements and shape functions. Figure (22) and (23) shows the distribution of the axial strains (ϵ_{yy}) and axial stresses (σ_{yy}) at the cross-section close to the fixed end because this is the area of maximum strains and stresses.

In order to check the accuracy of our model, the maximum stress obtained is compared with the NASTRAN model. The maximum stress range obtained from the NASTRAN model ranges from -0.0059 [MPa] to 0.0055 [Mpa] which is close to our model which has a stress range of -0.0033 [MPa] to 0.0033 [MPa].

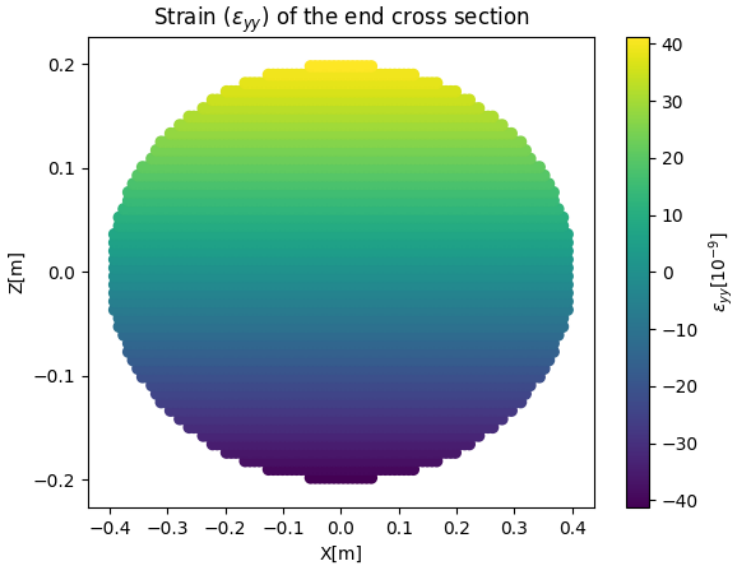

Figure 22: Distribution of axial strain at the fixed end cross-section (ϵ_{yy})

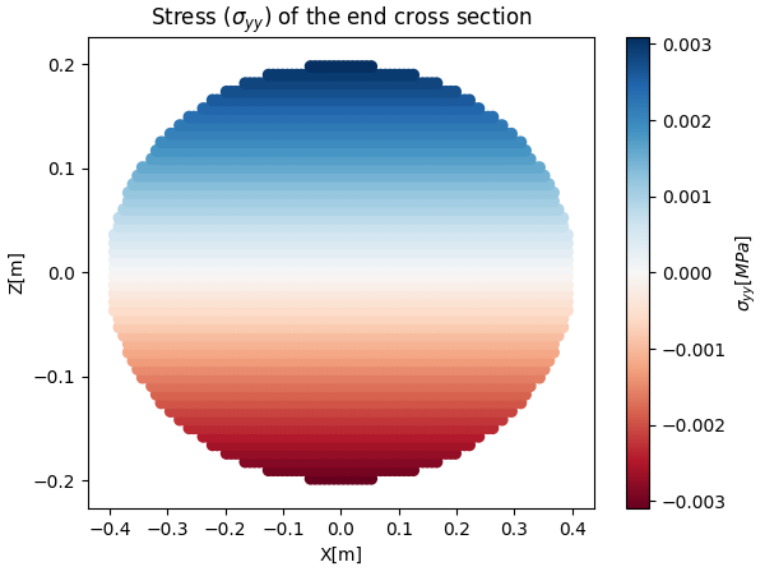

Figure 23: Distribution of axial stress at the fixed end cross-section (σ_{yy})

Figure (24) given below presents an elliptical beam model built using NASTRAN. It shows the range of maximum axial stress (σ_{yy}) at the cross-section close to the fixed end when subjected to a vertical load (P_{u_z}) of -100[N].

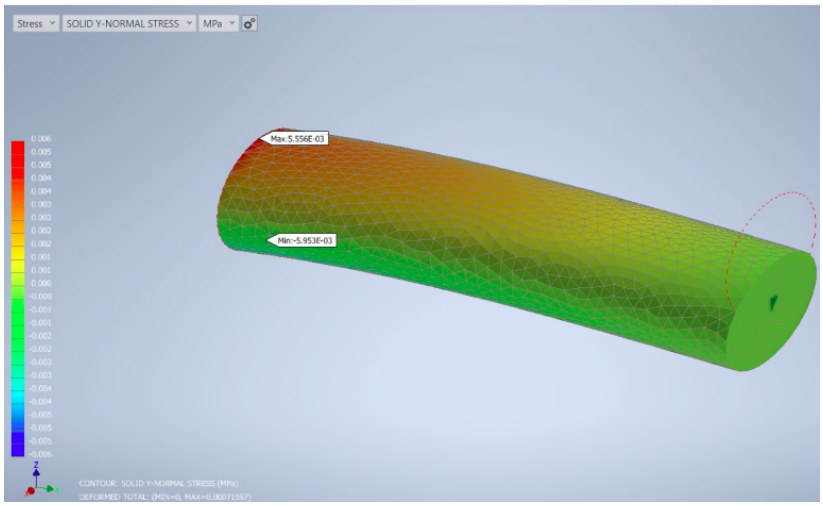

Figure 24: NASTRAN model showing the distribution of axial stress (σ_{yy})

Conclusion:

In the present work, finite element models with three different type of beam elements have been compared in the static analysis of beam structures using refined 1D beam models. Lagrange (L4) polynomials are chosen for the expansion across the cross-section. A square and an elliptical cross-section has been chosen for analysis and the results are compared with the reference solution from the literature and NASTRAN solution. The results show that

- The Refined 1D beam models are able to provide quasi-3D solution of the displacements and stress fields, which makes the model very impressive with respect to the classical beam models (like Euler-Bernoulli) which is not able to provide the stress fields
- The unknown variables are only displacements, no rotation or higher-order variables are required to describe the displacement or stress fields
- The Degrees of freedom (DOF) required for the analysis is far less compared to the DOF required for the beam models built using solid elements. For example the analysis of square cross-section beam using solid elements (NASTRAN) requires 25,857 DOFs but with refined beam elements (For 40 B3 elements and L4 expansion) it requires only 972 DOFs

In short, the models appear to be very impressive for the analysis of beam structures. These models provide a considerable amount of accuracy when compared to the commercial software but with a lower computational cost. Application to higher-order deformation like torsion as well as complex structures like aircraft wings, rotor blades etc and dynamics could be the subject of future research.

References

[1] E Carrera, G Giunta, P Nali, and M Petrolo. Refined beam elements with arbitrary cross-section geometries. *Computers & structures*, 88(5-6):283–293, 2010.

[2] Erasmo Carrera, Maria Cinefra, Marco Petrolo, and Enrico Zappino. *Finite element analysis of structures through unified formulation*. John Wiley & Sons, 2014.

[3] Erasmo Carrera, Gaetano Giunta, and Marco Petrolo. *Beam structures: classical and advanced theories*. John Wiley & Sons, 2011.

[4] Erasmo Carrera, Alfonso Pagani, and Marco Petrolo. Use of lagrange multipliers to combine 1d variable kinematic finite elements. *Computers & Structures*, 129:194–206, 2013.